Journal of Applied Engineering and Technological Science
Vol 6(2) 2025: 849-861

LARGE-SCALE PERIODIC GUST GENERATION AND SPECTRAL ANALYSIS APPROACH FOR CHARACTERIZATION AND EVALUATION

Berk Zaloglu[1]*, Oksan Cetiner[2]
Faculty of Aeronautics and Astronautics, Istanbul Technical University[12]
berk_zaloglu@yahoo.com

Received: 25 April 2024, Revised: 22 November 2024, Accepted: 14 January 2025
**Corresponding Author*

ABSTRACT
Generating a periodic continuous gust in a controlled manner and at sufficiently large scales for the gust encounter studies on MAV applications is a challenge. In order to achieve it a pitching and plunging flat-plate is utilized with aggressive motion profiles. A range of periodic functions in pitch and plunge axes are investigated for the motion of the gust generator. Significant and distinct vortices are measured with PIV in its wake. An in-depth spectral analysis of the velocity vector field of the wake is performed to investigate the generated gust characteristics since the aggressive motion profiles can produce uniform and/or weak gust characteristics. To obtain the cases that simulate large-scale transverse wind gusts in a quasi-sinusoidal pattern, the PIV results are evaluated by using auto- and cross-spectral density plots of the entire flow field at the wake, ensuring the consistency of the gust characteristics for future gust wing encounter studies. Four cases in which the flat-plate moves with the quasi-feathering condition provide gusts that are useful to employ in MAV gust studies.
Keywords: *Gust Generation, Characterization, MAV, PIV*

1. Introduction

The growing utilization of micro aerial vehicles (MAVs) in aviation, underlines the significance of comprehending the gust effects on their aerodynamics. Due to their low Reynolds number flight envelope and small size, MAVs are particularly vulnerable to gusts. Ensuring their stability in gusty conditions is crucial, especially when peak gust velocities correspond to a significant portion of the MAV's airspeed (Viswanath & Tafti, 2010). Watkins et al. (2006) highlighted atmospheric turbulence as a major challenge for MAVs due to the relative size of vortices and eddies in comparison to the dimensions of MAVs. However experimental studies in this area have been limited, primarily due to the challenge of simulating controllable, uniform, and continuous gusts which are strong enough for MAV applications.

NACA initiated studies on the effects of gusts, focusing on analytically exploring the loads imposed on airplanes by atmospheric turbulence (Hunsacker & Wilson, 1915). Roadman & Mohseni (2009) stated that at the beginning of analytical gust modeling, the focus was on the discrete gusts in which a single finite change in velocity is accounted for. Over time, the treatment of the gust problem transitioned from discrete gusts to investigating the continuous nature of turbulence (Murrow et al., 1989). Consequently, both discrete gust and spectral gust analyses are utilized in aircraft design (Fuller, 1997). The von Karman and Dryden models that are generally utilized as the atmospheric disturbance models for traditional aircrafts are inadequate for MAVs that interact with complex velocity fields (Zarovy et al., 2010).

The experimental studies on continuous gust focused on isotropic, homogenous turbulence mostly explored by utilizing passive grids (Roadman & Mohseni, 2009). The works of Comte-Bellot & Corrsin (1966, 1971) pioneer this methodology in which wired grids are employed to generate isotropic homogeneous turbulence. Watkins et al., (2010) achieved to generated well-mixed turbulent flows applicable to MAV applications by combining grids and screens in a wind tunnel. However, passive grids have limitations in adjusting turbulence levels, as the length scale of turbulence is tied to the mesh spacing for a given velocity; in contrast, active grids have the capability to manipulate turbulence levels for specific flow velocity and can generate larger length scales than passive grids (Roadman & Mohseni, 2009). Pioneering the active grid turbulence generators, Makita (1991) utilized a design consisting of vertical and horizontal oscillating diamond-shaped wings. Another method for gust generation commonly used in wind tunnels is the oscillating vanes mechanism (Smith, 2018). It

was first used by Garby et al. (1957), and later Reid & Wrestler (1961) used a couple of oscillating semi-span vanes. Buell employed harmonically pitching vanes to explore spanwise gust. The external-jet method is utilized mostly for discrete gust generation. (Perrotta & Jones (2016, 2017) resort to a set of jets to generate a zone of transverse velocity in a water tow tank. Yet another way of producing gust is to position a moving airfoil upstream of the test section. Hakkinen & Richardson (1957) employed a plunging airfoil shedding vortices for the NASA gust test system. Similarly, Neumann and Mai (2013) and Klein et al. (2015) employed a single-pitching airfoil positioned upstream of a test model as a gust generator. The resulting vortical gust disturbances have low intensity compared to the freestream, inducing a narrow band wake in the flow field. Hufstadler and McKeon (2019) explored a single flat-plate undergoing either pure pitching or pure plunging motion as a discrete vortex gust generator. They noted that neither method was ideal for generating isolated gusts, suggesting a combination of pitching motion and plunging motion as a potential solution. Similarly, Wei et al. (2019b) investigated a single airfoil gust generator with the aim of generating sinusoidal transverse gusts; they observed that the streamwise fluctuations were approximately one-third the amplitude of transverse velocity fluctuations. Limitations in their experimental setup prevented detailed analysis of the gust profile downstream and off-axis from the measurement point.

Over the last twenty years, several numerical studies have been conducted to examine the effects of gusts on MAVs, including studies by Lian & Shyy (2007), Viswanath & Tafti (2010), and Jones & Yamaleev (2012). In contrast, experimental research on this topic has been relatively limited. One of the key challenges has been the complexity of providing a controlled, uniform periodic gust in sufficient strength to be relevant for MAV studies. Wind tunnel and water channel layouts normally intend to minimize turbulence intensity and velocity fluctuations. Yet such controlled conditions differ marginally from the MAVs' typical operation conditions with large-scale gust encounters. As described in the gust overview study of Jones & Cetiner (2021), a transverse gust occurs when an airfoil passes through an updraft or a strong shear layer which usually comes across as a weather phenomenon and large-scale wakes in urban environments, and other complex terrain.

The current study aims to produce active-generated periodic continuous transverse gusts with a proposed approach for the characterization and evaluation of the generated gusts concentrated upon applications for gust encounters of MAVs. A flat-plate undergoing periodic motion in pitching and plunging is utilized to produce distinct vortices in its wake, simulating transverse quasi-sinusoidal gusts, as introduced in our previous work (Biler et al., 2015; Engin et al., 2018). The same gust generation system is used in the discrete gust encounter investigation of Biler et al. (2021) which was also included in the review paper of Jones et al. (2022). While the gust generator design and motion profiles in this study aim to induce strong large-scale gusts by more intense excitation of the flow field, this demand may potentially cause irregular vortex shedding in the near wake. Our proposed gust evaluation approach addresses this complication by examining the entire flow field instead of a point or a line in the wake of the gust generator. In-depth spectral analysis of the DPIV measurements taken in the wake of the gust generator enables gust characterization. This approach provides a comprehensive understanding of the generated gust and facilitates the generation of gust with desired characteristics to reliably investigate continuous gust encounters with airfoils for future MAV application experiments.

2. Experimental Setup and Methodology

The experiments are carried out in the water channel at Trisonic Laboratories of Istanbul Technical University. It is a free-surface, large-scale, closed-circuit, water channel with a test section having cross-sectional dimensions of 1010mm x 790mm. A flat-plate made of Plexiglas is used as the gust generator. The flat-plate has a span of 400mm, a chord (c) of 100mm, and a thickness of 5mm; both of its edges are beveled at 30°. It is mounted to a connection rod at its half-chord in a vertically cantilevered setup. This setup for the gust generator is chosen specifically to let the leading and trailing edges be interchangeable during the continuous motion. The connection rod joins the flat-plate to a servo motor (Kollmorgen AKM33E) providing the pitch motion with a Danaher Motion S300 servo controller. This pitching motor is

placed on a linear table providing the plunge motion with a servo motor (Kollmorgen AKM54K) run via Danaher Motion ServoSTAR S700 servo controller. The pitch and plunge motions of the flat-plate have an accuracy of 0.15º and 0.0104m respectively as indicated in the studies of Son & Cetiner (2017, 2018) in which the same setup was employed. Motor motion profiles fed to the servo controllers are generated by a signal generator coded in Labview. A rectangular end plate with a 30° bevel is positioned above the channel to reduce the free-surface effects.

A Particle Image Velocimetry (PIV) acquisition system is employed to obtain the vector fields at the wake of the oscillating flat-plate used as the gust generator. The flow field is illuminated by a dual cavity Nd:Yag laser. 10μm diameter silver-coated glass spheres are used for seeding the water. A couple of 10-bit cameras with 1600×1200 pixels resolution are stationed under the water channel. By an in-house code, the two double-frame images captured by the camera couple are merged. The obtained PIV images are processed by a double-frame, cross-correlation technique. The window size of the interrogation is 64×64 pixels with an overlapping 50% in each direction. The resulting velocity field has a grid resolution of 3.2mm × 3.2mm at the flow plane with a total of 3264 velocity vectors. The data acquisition is triggered with the gust generator's third motion cycle to allow a fully developed gust flow. The signal generator VI also triggers the PIV data acquisition system, National Instruments PCI-6601 timer device is utilized for the synchronization of the PIV system with the motion system. In each case, data is captured with a 4Hz sampling rate to a total of 400 velocity vector fields. The same PIV system was employed in the study of Biler et al. (2021) and a maximum PIV uncertainty of 0.2 percent was found. The experimental setup is demonstrated in Fig. 1.

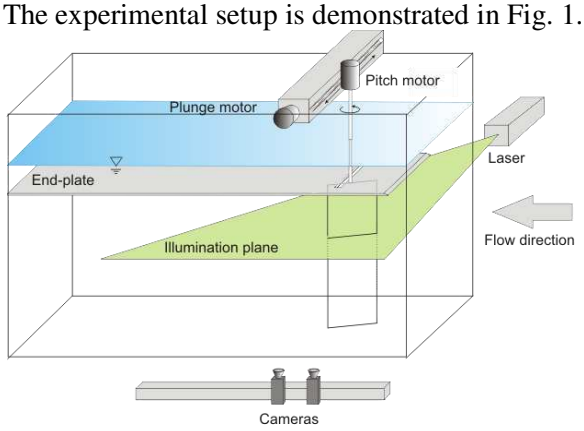

Fig. 1. Experimental Setup.

3. Experimental Parameters

The flat-plate undergoes pitching and plunging motions defined with the following equations:

$$\alpha(t) = \alpha_{offset} + \alpha_{amp}\cos(2\pi ft)$$

$$h(t) = h_{amp}\sin(2\pi ft)$$

where $h(t)$ is the linear plunge motion, normal to the freestream velocity, $\alpha(t)$ is the angular pitch motion. h_{amp} is the plunge amplitude, α_{amp} is the pitch amplitude and α_{offset} is the angle of attack offset. f is the flapping frequency, as the same for both plunge and pitch motions.

Both linear and sinusoidal motions are investigated; for the pitching motion, the flat-plate follows either a square or a cosine signal and for the plunge motion, it follows a triangle or sine signal. The flat-plate is intended to be in feathering motion to conform with the minimum possible energy addition into the flow. The amplitude of the plunge motion, h_{amp} is calculated according to the frequency and the pitch amplitude for feathering conditions. Because of the real-world acceleration limitations of the experimental system, the triangle and square signals are smoothed as demonstrated in Fig. 2. The flat-plate is in a quasi-feathering motion in sinusoidal cases in order to keep the same plunge amplitude as the linear cases.

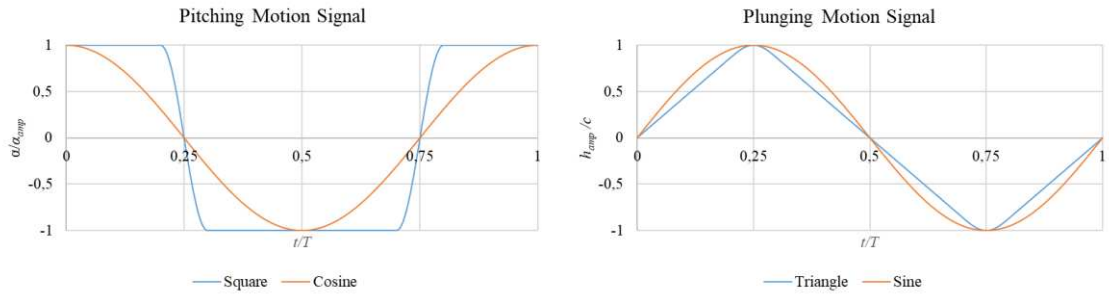

Fig. 2. Pitching and plunging motion signals.

The investigated motion parameters are given in Table 1. The water channel velocity is set to have a Reynolds number of 10000 for all cases. High angle of attack values are investigated for the purpose of generating large-scale gusts spanning in a wide wake in the transverse direction. With the intention of generating strong vortices at the apices of the plunge motion, the flat-plate makes a half- or a full-revolution roll in some cases manifesting with non-zero α_{offset} values. Because of the flat-plate's shape and center of rotation, these rolls do not change the symmetry of the motion.

Table 1 - The gust generating flat-plate's motion parameters.

Case	f [Hz]	α_{offset} [deg]	α_{amp} [deg]	h_{amp}/c	Pitch	Plunge
1	0.25	0	45	N/A	Square	N/A
2	0.5	0	45	0.5	Cos	Sin
3	0.25	0	45	1	Square	Triangle
4	0.25	0	45	1	Cos	Sin
5	0.25	0	30	N/A	Square	N/A
6	0.5	0	30	0.29	Cos	Sin
7	0.25	0	30	0.58	Square	Triangle
8	0.25	0	30	0.58	Cos	Sin
9	0.25	90	-45	1	Square	Triangle
10	0.25	90	-45	1	Cos	Sin
11	0.25	90	-60	0.58	Square	Triangle
12	0.25	90	-60	0.58	Cos	Sin
13	0.25	180	-135	1	Square	Triangle
14	0.25	180	-135	1	Cos	Sin
15	0.25	180	-150	0.58	Square	Triangle
16	0.25	180	-150	0.58	Cos	Sin
17	0.25	-180	225	1	Square	Triangle
18	0.25	-180	225	1	Cos	Sin
19	0.25	-180	210	0.58	Square	Triangle
20	0.25	-180	210	0.58	Square	Triangle

4. Gust Characterization and Evaluation Approach

The main focus of the current study is to obtain periodical uniform transverse gusts on a scale large enough to simulate flight conditions for MAVs and with minimum streamwise effects. Therefore, the prospect of the generated flow is to have uniform and nominally sinusoidal transverse velocity fluctuations, $v'(t)$ with a mean transverse velocity, $\bar{v}$ near zero. Whereas the streamwise velocity fluctuation, $u'(t)$ is minimal and the mean streamwise velocity, $\bar{u}$ stays in the range of the freestream velocity, U_∞. Furthermore, the phase of the transverse velocity fluctuations is taken into consideration, so that the phase shift is required to be transversely uniform along the streamwise direction. The equations defining the flow are presented below where u and v are the streamwise and transverse velocities, respectively.

$$u(t) = \bar{u} + u'(t)$$

$$v(t) = \bar{v} + v'(t)$$

In Fig. 3, the position of the gust generator is visualized with respect to the measured DPIV velocity field; the center of rotation is at x/c=−0.5, and the origin of the plunge motion is at y/c=0.6. The velocity field data go under a three-phase evaluation of spectral analysis to eliminate the cases that do not satisfy the aforementioned criteria. Starting with the

determination of the predominant frequencies, auto-spectral and cross-spectral analyses of the velocity fluctuations are carried out to obtain contour plots of the amplitude of the auto-spectral density, |S(f)| and phase angle, φ(f) of the entire flow field, respectively. This technique is employed in many former flow-induced vibration studies (Ekmekci & Rockwell, 2003, 2007, 2010; Fu & Rockwell, 2005).

4.1 Determination of the Predominant Frequencies

The first step is to determine the predominant frequency, f_0 of the fluctuations for each velocity component. For each investigated case, eight points are selected to probe the streamwise and transverse velocity components of the DPIV velocity field data at 400 instances in time (Fig. 3). Four of those points are chosen on the symmetry line of the motion, in other words, the centerline of the flow, namely y/c=0.6, and the other four points are aligned on y/c=1 with all apart from each other with a distance of x/c=0.6. The near wake of the gust generator (x/c<0.5) is omitted in the evaluation and the characterization study takes into account a region sufficiently away from the gust generator's trailing edge where an airfoil will be present for future gust-encounter experiments.

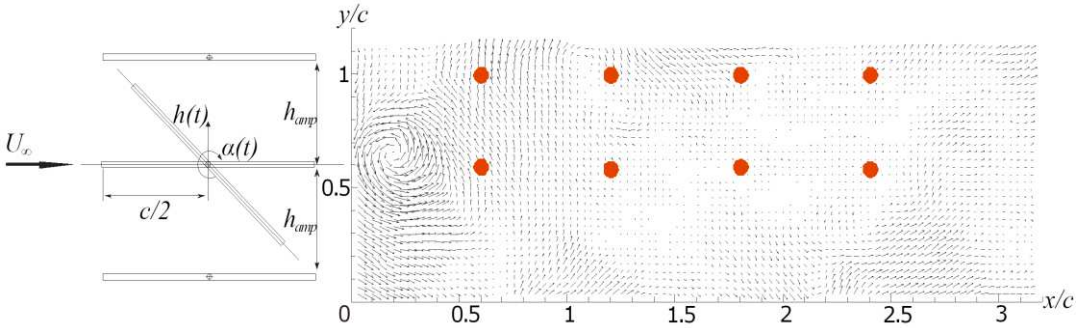

Fig. 3. Kinematics of The Gust Generator And The Eight Velocity Probe Points (Red Dots).

The velocity data with the sampling rate of 4Hz taken for a duration of 10 seconds is well above the Nyquist criterion for the flat-plate's motion frequency, even enough to visualize in detail a full cycle of motion. The predominant frequency is expected to be equal to or multiple of that motion frequency. FFT is performed on the dataset by using MATLAB at each of the eight probe points for both streamwise and transverse components. The resulting frequency spectrum of each signal reveals the velocity fluctuations' predominant frequency in the flow field as presented in Fig. 4.

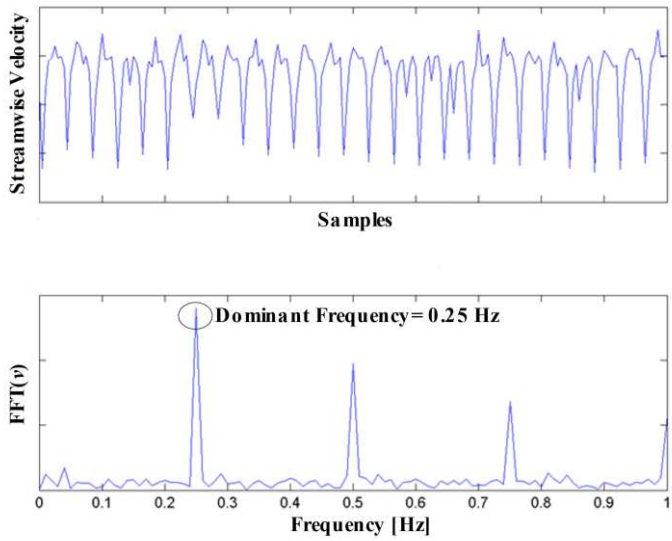

Fig. 4. Velocity probe data and FTT of the streamwise velocity of Case 1.

The reduced frequency, k is used to non-dimensionalize the frequency of the periodic gust as in recent studies (Wei et al., 2019a; 2019b; Young & Smyth, 2021). This parameter

represents the size of the gust in time scale with respect to the size of the airfoil and is expressed as,

$$k = \pi f_0 c / U_\infty$$

4.2 Auto- and Cross-Spectral Analysis

The second and most distinctive phase of the evaluation process is the calculation of the auto- and cross-spectral analysis. The definition and calculation procedure of auto-spectral density, S_{xx}, and cross-spectral density, S_{xv} can be found in Newland (2005), defined as below:

$$S_{xx}(\bar{\omega}) = \frac{1}{2\pi}\int_{-\infty}^{\infty} R_{xx}(\tau) e^{-i\omega t} d\tau$$

$$S_{xy}(\bar{\omega}) = \frac{1}{2\pi}\int_{-\infty}^{\infty} R_{xy}(\tau) e^{-i\omega t} d\tau$$

where R_{xx} and R_{xv} are the auto- and cross-correlation functions defined as:

$$R_{xx}(\bar{\omega}) = \frac{1}{N}\sum_{n=1}^{N} x_n(t) x_n(t+\tau)$$

$$R_{xy}(\bar{\omega}) = \frac{1}{N}\sum_{n=1}^{N} x_n(t) y_n(t+\tau)$$

Auto-spectral density is basically the Fourier transform of the autocorrelation function or in other words a normalized version of the auto power spectrum, whereas the cross-spectral density is the Fourier transform of the cross-correlation function. Auto-spectral density provides the means to determine the coherence of periodic fluctuations of velocity at a single point (Sever, 2005). Auto-spectral density, $S(f_0)$ of the streamwise and transverse velocity component at each grid point of the velocity vector field for the predominant frequency is evaluated as the first step. A representative schematic of the auto-spectrum is shown in Fig. 5, the amplitude of the peak at the predominant frequency, f_0 is indicated as $|S_v(f_0)|$ for the transverse velocity component. The same definition is valid for the streamwise component $|S_u(f_0)|$.

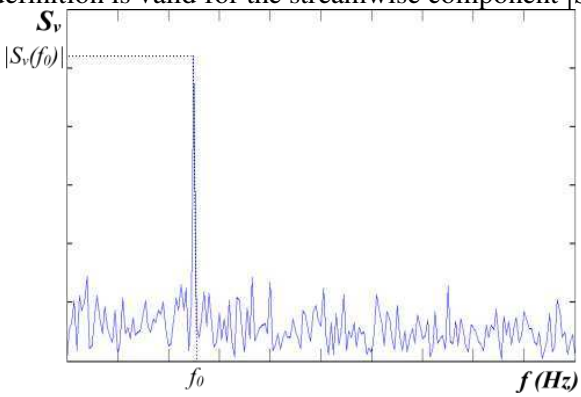

Fig. 5. The auto-spectrum of The Transverse Velocity Component and The Amplitude of The Peak Value at The Predominant Frequency.

Contours of these peak amplitudes are obtained for the whole flow field. The application of this technique is explained in Fig. 6 of Ekmekci and Rockwell (Ekmekci & Rockwell, 2010). As Ekmekci (Ekmekci, 2002) stated features of the unsteady flow field can be represented by the patterns of auto-spectral density contours at the predominant frequency. The plots containing the contours of the constant peak amplitude of auto-spectral density, $|S_u(f_0)|$ and $|S_v(f_0)|$ of streamwise and transverse velocity fluctuations respectively are presented in Fig. 6.

These plots show the intensity distribution of the fluctuations' magnitude for the predominant frequency, basically presenting how powerful is the generated gust throughout the flow field.

Since it is aimed to generate transverse gusts, the cases that have a greater or equal amplitude of streamwise fluctuations than that of transverse fluctuations are eliminated at this stage. An example of such is Case 19 (Fig. 6), where the amplitudes of transverse and streamwise fluctuations are approximately at the same level. In most of the investigated cases, it is observed that the transverse fluctuations around the centerline of the flow field are strong; however, they generally get weaker downstream and away from the centerline. Inversely, the streamwise fluctuations are weakest around the centerline of the flow field.

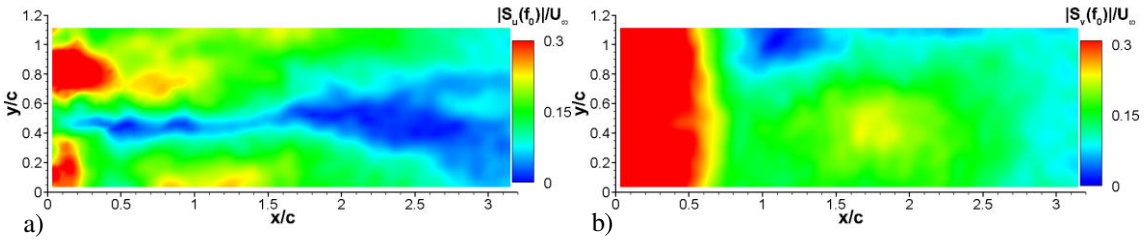

Fig. 6. The constant peak amplitude contours of auto-spectral density of a) streamwise b) transverse velocity fluctuations of Case 19.

The next stage is the cross-spectral analysis involving a velocity component at two points, to determine the magnitude and phase angle at a given frequency. For determining the nature of the propagating disturbance along the wake of the flat-plate, the cross-spectral analysis is accomplished using the same overall technique as for the auto-spectral analysis. The reference grid point (x/c=0.1, y/c=0.6) for the cross-spectral analysis is located at the centerline of the plunge motion just behind the trailing edge of the gust-generating flat-plate. This analysis of the streamwise and transverse velocity fluctuations at the predominant frequency at each grid point over the entire flow field, provides the contours of the constant phase angle $\Phi_u(f_0)$ and $\Phi_v(f_0)$, respectively.

These contour plots demonstrate the shifting of the constant phase angle, $\Phi(f_0)$ of a fluctuation throughout the velocity field. Since it is desired to have a uniform shifting downstream, the cases with a disordered or uneven change of phase angle along the flow field are eliminated. An example of undesired phase shifting is Case 1, as seen in Fig. 7, the crooked contours and erratic changes in phase angle do not represent a wavefront for a sinusoidal gust.

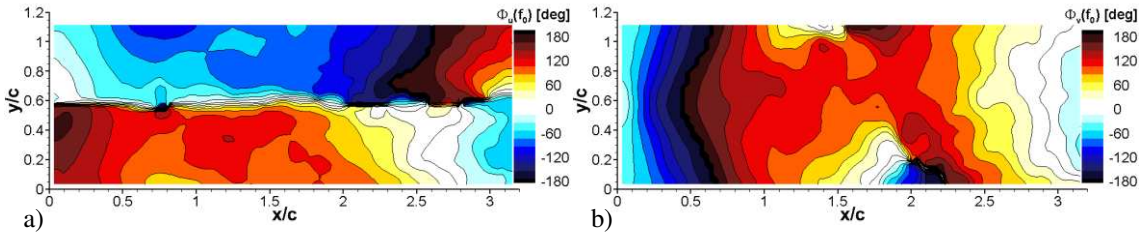

Fig. 7. The Constant Phase Angle Contours For The Predominant Frequency Of a) Streamwise b) Transverse Velocity Fluctuations Of Case 1.

5. Results and Discussions

After the elimination process, four gust cases met the selection criteria (Table 2). These gusts have much weaker streamwise fluctuations compared to transverse fluctuations. Thus, the cases can simulate a transverse gust. Also, their characteristics span over an area wide enough to position a test model for future studies.

Table 2 - Reduced Frequencies of Selected Gusts And Motion Parameters of The Gust Generator.

Gust	k	f [Hz]	α_{offset} [deg]	α_{amp} [deg]	h_{amp}/c
A	1.57	0.5	0	45	0.5
B	0.785	0.25	0	45	1.0
C	0.785	0.25	180	-135	1.0
D	0.785	0.25	90	-60	0.58

Fig. 8 demonstrates the contours of the constant peak amplitude of auto-spectral density of Gust A. Streamwise velocity fluctuations are fairly weak. In contrast, strong and persistent

transverse fluctuations are present with almost twice the intensity of streamwise fluctuations even away from the centerline. The predominant frequency of the fluctuations is 0.5Hz, the same as the gust generator's motion frequency.

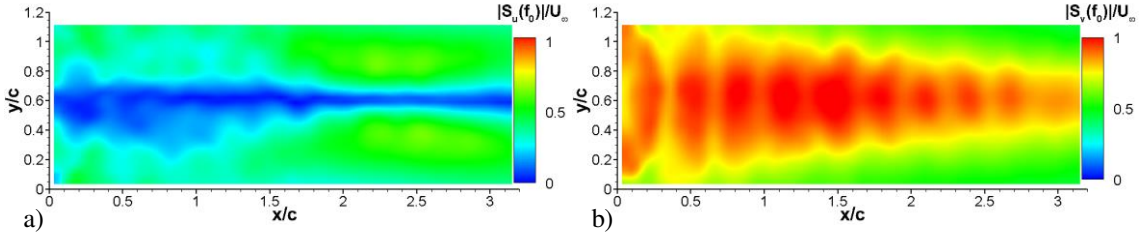

Fig. 8. The Constant Peak Amplitude Contours of Auto-Spectral Density of a) streamwise b) transverse velocity fluctuations of Gust A.

In Gusts A and B, the flat-plate moves with a maximum angle of attack of 45° and without any rolling motion. In Gust C, the flat-plate makes full-revolution backward rolls during the upstroke and downstroke while still reaching an angle of attack of ±45° at the centerline similar to the other two cases. In all selected cases, the predominant frequency is measured the same as the flat-plate's motion frequency. In Gust D, the flat-plate makes half-revolution backward rolls with an angle of attack of ±30° at the centerline.

Although Gust B, C, and D have the same predominant frequency of 0.25Hz, according to the contour plots of the peak amplitude of auto-spectral density, Gust B is weaker than others (Fig. 9 and 10, 11). On the other hand, Gust A constitutes another example of a gust reaching high amplitude fluctuations with a different predominant frequency.

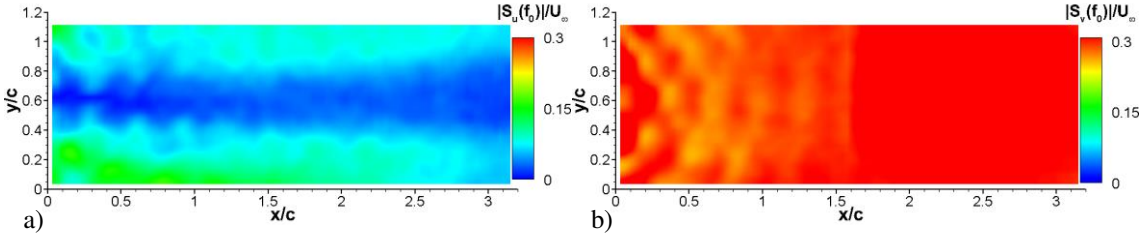

Fig. 9. The Constant Peak Amplitude Contours of Auto-Spectral Density of a) streamwise b) transverse velocity fluctuations of Gust B.

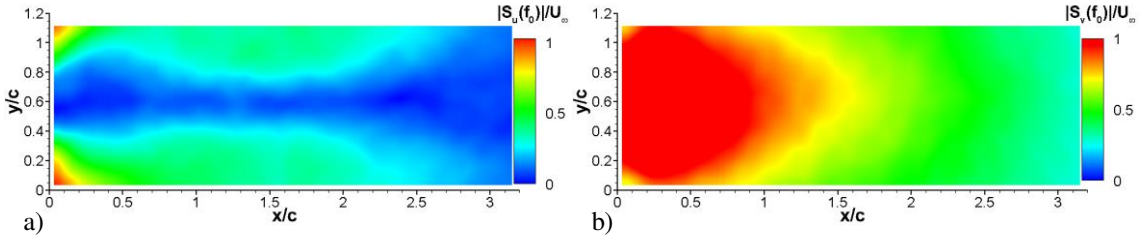

Fig. 10. The Constant Peak Amplitude Contours of Auto-Spectral Density of a) streamwise b) transverse velocity fluctuations of Gust C.

Gust C and Gust D demonstrated similar plots for transverse velocity with strong fluctuations consistent till x/c=1.5; even downstream from this point, the fluctuations are stronger in the transverse direction than streamwise (Fig. 10 and 11). The reason for this similarity might be caused by the backward rolls in pitching motion. However transverse fluctuations are stronger in Gust C most probably due to the higher angle of attack in its motion profile.

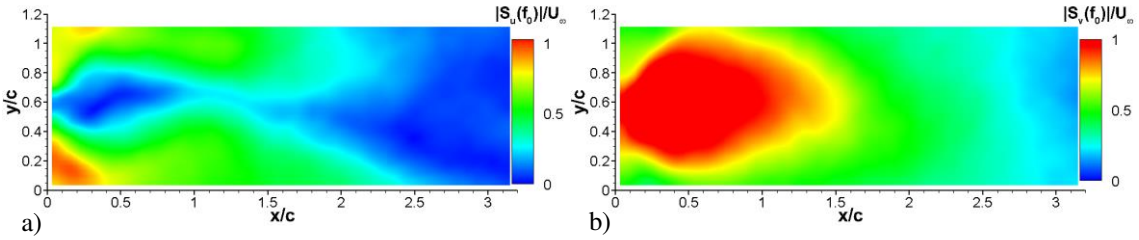

Fig. 11. The Constant Peak Amplitude Contours of Auto-Spectral Density of a) streamwise b) transverse velocity fluctuations of Gust D.

Figures 12, 13, 14, and 15 represent the contours of the phase angle of streamwise, $\Phi_u(f_0)$, and transverse $\Phi_v(f_0)$ fluctuations for Gust A, B, C, and D respectively. For the transverse velocity component, the phase angle shifts in almost parallel lines in the transverse direction throughout the flow field, indicating that a uniform wavefront approach to a model downstream will exist in future gust encounter studies. In all four cases, there is a similar phase angle difference of streamwise fluctuations between the upper and lower part of the flow field. However, in the case of Gust A the contours are much less skewed than others, probably due to its higher predominant frequency. Also, Gust A has a faster change of phase angle along the flow field. Especially Gust B, and C exhibit wider bands of change in the contours of the constant phase angle, evident in the transverse velocity fluctuations.

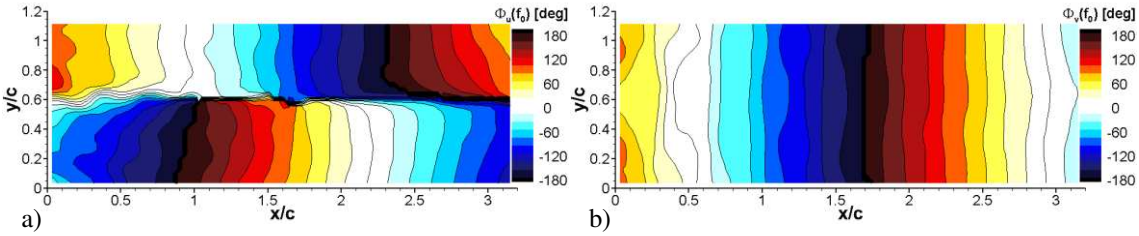

Fig. 12. The Constant Phase Angle Contours for The Predominant Frequency of a) streamwise b) transverse velocity fluctuations of Gust A.

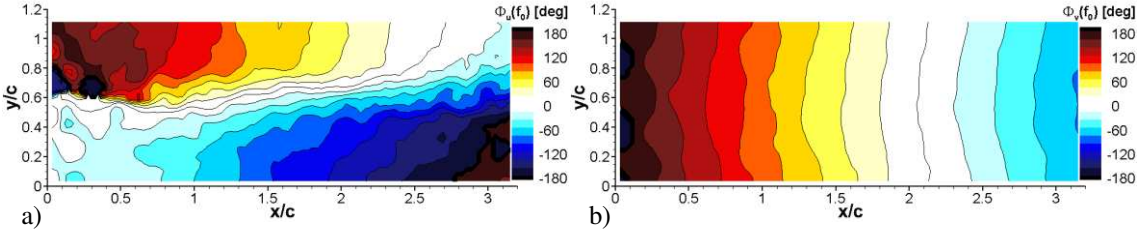

Fig. 13. The Constant Phase Angle Contours for The Predominant Frequency of a) streamwise b) transverse velocity fluctuations of Gust B.

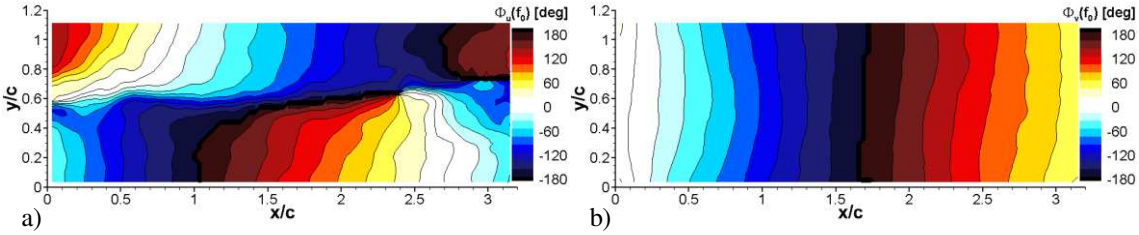

Fig. 14. The Constant Phase Angle Contours for The Predominant Frequency of a) streamwise b) transverse velocity fluctuations of Gust C.

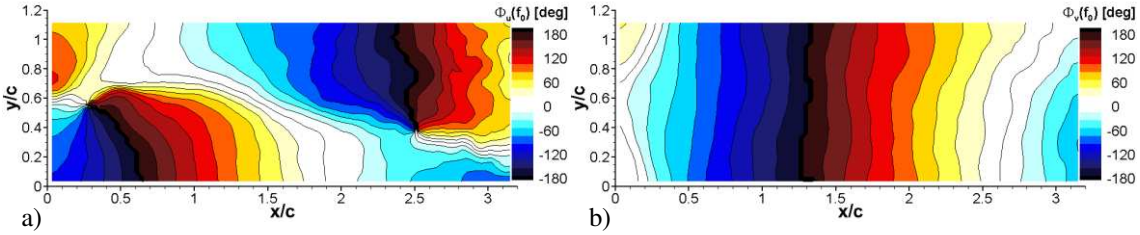

Fig. 15. The Constant Phase Angle Contours for The Predominant Frequency of a) streamwise b) transverse velocity fluctuations of Gust D.

To sum up, all four cases demonstrate a strong large-scale traverse periodic gust with minimal streamwise effects. The wavefronts of these gusts demonstrate a uniform shift along the flow field. The higher frequency motion of the gust generator at Gust A results in a faster phase shift and a longer area of strong gust influence. Gust B with its softer motion profile without any backward rolls and with a lower frequency demonstrates the weakest gust between the four cases, however, the area of influence is the largest and the most uniform. With similar motion profiles of backward rolls, the area of influence and gust strength of Gust C and D show up to be very similar with Gust C being the stronger of the two cases.

6. Conclusion

A pitching and plunging flat-plate wing is used to generate large-scale periodic continuous gusts. A detailed spectral analysis of the velocity vector field undertaken for the characterization revealed that the experimental setup successfully generates large-scale transverse quasi-sinusoidal gusts. Furthermore, the generated continuous gust affects the wake in a large transverse band, allowing for future gust-encounter investigations of wings at high angles of attack. This proves that the quasi-feathering condition of the flat-plate in sinusoidal motion is capable of producing the desired gust characteristics. Also, it is observed that the frequencies of the generated gusts are equal to the flat-plate's motion frequencies.

Unlike the general approach in studies on the subject, the characterization examines the whole flow field in the wake of the gust generator instead of a point or a line (Hakkinen & Richardson, 1957; Jancauskas & Melbourne, 1980; Saddington et al., 2015; Wei et al., 2019a; 2019b; Olson et al., 2021). The spectral analyses give a complete picture of the flow field in the wake of the flapping flat-plate. The evaluation of the auto-spectral and cross-spectral analyses ensures the quality of the perturbations spreading over a large area in the wake of the gust generator which is not possible in the classical one-point approach. Therefore, the desired characteristics and quality of the generated gust can be accomplished in a much more reliable manner in experimental gust studies. The selected gusts in this study were already comparatively investigated in the 7th Chapter of the NATO STO (2020) report of STO-TR-AVT-282. The investigation of the gust velocity profiles in the region of a wing encounter will be helpful in future work for wing gust encounter studies.

Acknowledgment

The authors acknowledge the funding provided by the Scientific and Technological Research Council of Turkey (TUBITAK) Grant 112M682 and the Scientific Research Projects Department of Istanbul Technical University (Project Number: 1652-37334).

References

Biler, H., Sedky, G., Jones, A. R., Saritas, M., & Cetiner, O. (2021). Experimental investigation of transverse and vortex gust encounters at low Reynolds numbers. *AIAA Journal*, *59*(3), 786–799.

Biler, H., Zaloglu, B., & Cetiner, O. (2015). Effect of Spanwise Gust on a Wing. *8th Ankara International Aerospace Conference*, 10–12. http://aiac.ae.metu.edu.tr/paper.php/AIAC-2015-118

Comte-Bellot, G., & Corrsin, S. (1966). The use of a contraction to improve the isotropy of grid-generated turbulence. *Journal of Fluid Mechanics*, *25*(4), 657–682. https://doi.org/10.1017/S0022112066000338

Comte-Bellot, G., & Corrsin, S. (1971). Simple Eulerian time correlation of full-and narrow-band velocity signals in grid-generated, 'isotropic' turbulence. *Journal of Fluid Mechanics*, *48*(2), 273–337. https://doi.org/10.1017/S0022112071001599

Ekmekci, A. (2002). *Self-excited oscillations of free-and bonded-shear flow past a resonant cavity* [PhD Thesis]. Lehigh University.

Ekmekci, A., & Rockwell, D. (2003). Self-sustained oscillations of shear flow past a slotted plate coupled with cavity resonance. *Journal of Fluids and Structures*, *17*(8), 1237–1245. https://doi.org/10.1016/S0889-9746(03)00073-2

Ekmekci, A., & Rockwell, D. (2007). Oscillation of shallow flow past a cavity: Resonant coupling with a gravity wave. *Journal of Fluids and Structures*, *23*(6), 809–838. https://doi.org/10.1016/j.jfluidstructs.2006.12.005

Ekmekci, A., & Rockwell, D. (2010). Effects of a geometrical surface disturbance on flow past a circular cylinder: A large-scale spanwise wire. *Journal of Fluid Mechanics*, *665*, 120–157. https://doi.org/10.1017/S0022112010003848

Engin, K., Aydin, E., Zaloglu, B., Fenercioglu, I., & Cetiner, O. (2018). Large scale spanwise periodic vortex gusts or single spanwise vortex impinging on a rectangular wing. *2018 Fluid Dynamics Conference*, 3086. https://doi.org/10.2514/6.2018-3086

Fu, H., & Rockwell, D. (2005). Shallow flow past a cylinder: Control of the near wake. *Journal of Fluid Mechanics*, *539*, 1–24. https://doi.org/10.1017/S0022112004002666

Fuller, J. R. (1997). Evolution and future development of airplane gust loads design requirements. *1997 World Aviation Congress*, 5577. https://doi.org/10.2514/6.1997-5577

Garby, L. C., Kuethe, A. M., & Schetzer, J. D. (1957). *The generation of gusts in a wind tunnel and measurement of unsteady lift on an airfoil* (Vol. 57). Wright Air Development Division, Air Research and Development Command ….

Hakkinen, R. J., & Richardson Jr, A. S. (1957). *Theoretical and experimental investigation of random gust loads Part I: Aerodynamic transfer function of a simple wing configuration in incompressible flow* (NACA-TN-3878). National Advisory Committee for Aeronautics.

Hufstedler, E. A. L., & McKeon, B. J. (2019). Vortical gusts: Experimental generation and interaction with wing. *AIAA Journal*, *57*(3), 921–931. https://doi.org/10.2514/1.J056914

Hunsacker, J. C., & Wilson, E. B. (1915). *Report on behaviour of aeroplanes in gust turbulence* (NACA TR-1 (MIT)). National Advisory Committee for Aeronautics.

Jancauskas, E., & Melbourne, W. (1980). The measurement of aerodynamic admittance using discrete frequency gust generation. *Australasian Conference on Hydraulics and Fluid Mechanics (7th: 1980: Brisbane, Qld.)*, 70–73.

Jones, A. R., & Cetiner, O. (2021). Overview of unsteady aerodynamic response of rigid wings in gust encounters. *AIAA Journal*, *59*(2), 731–736. https://doi.org/10.2514/1.J059602

Jones, A. R., Cetiner, O., & Smith, M. J. (2022). Physics and modeling of large flow disturbances: Discrete gust encounters for modern air vehicles. *Annual Review of Fluid Mechanics*, *54*, 469–493. https://doi.org/10.1146/annurev-fluid-031621-085520

Jones, M., & Yamaleev, N. (2012). The effect of a gust on the flapping wing performance. *50th AIAA Aerospace Sciences Meeting Including the New Horizons Forum and Aerospace Exposition*, 1080. https://doi.org/10.2514/6.2012-1080

Klein, S., Hoppmann, D., Scholz, P., & Radespiel, R. (2015). High-lift airfoil interacting with a vortical disturbance: Wind-tunnel measurements. *AIAA Journal*, *53*(6), 1681–1692. https://doi.org/10.2514/1.J053441

Lian, Y., & Shyy, W. (2007). Aerodynamics of low Reynolds number plunging airfoil under gusty environment. *45th AIAA Aerospace Sciences Meeting and Exhibit*, 71. https://doi.org/10.2514/6.2007-71

Makita, H. (1991). Realization of a large-scale turbulence field in a small wind tunnel. *Fluid Dynamics Research*, *8*(1–4), 53. https://doi.org/10.1016/0169-5983(91)90030-M

Murrow, H., Pratt, K., & Houbolt, J. (1989). NACA/NASA research related to evolution of US gust design criteria. *30th Structures, Structural Dynamics and Materials Conference*, 1373. https://doi.org/10.2514/6.1989-1373

NATO STO. (2020). *Unsteady Aerodynamic Response of Rigid Wings in Gust Encounters* (STO-TR-AVT-282). https://www.sto.nato.int/publications/STO%20Technical%20Reports/STO-TR-AVT-282/$$TR-AVT-282-ALL.pdf

Neumann, J., & Mai, H. (2013). Gust response: Simulation of an aeroelastic experiment by a fluid–structure interaction method. *Journal of Fluids and Structures*, *38*, 290–302. https://doi.org/10.1016/j.jfluidstructs.2012.12.007

Newland, D. E. (2005). Digital spectral analysis I: Discrete Fourier transforms. In *An Introduction to Random Vibrations, Spectral & Wavelet Analysis* (Third Edition, pp. 113–124). Dover Publications.

Olson, D. A., Naguib, A. M., & Koochesfahani, M. M. (2021). Development of a low-turbulence transverse-gust generator in a wind tunnel. *AIAA Journal*, *59*(5), 1575–1584. https://doi.org/10.2514/1.J059962

Perrotta, G., & Jones, A. R. (2016). Transient aerodynamics of large transverse gusts and geometrically similar maneuvers. *54th AIAA Aerospace Sciences Meeting*, 2074.

Perrotta, G., & Jones, A. R. (2017). Unsteady forcing on a flat-plate wing in large transverse gusts. *Experiments in Fluids*, *58*(8), 1–11. https://doi.org/10.1007/s00348-017-2385-z

Reid, C. F., & Wrestler, C. (1961). *An investigation of a device to oscillate a wind-tunnel airstream* (Technical Note D-739). NASA.

Roadman, J., & Mohseni, K. (2009). Gust characterization and generation for wind tunnel testing of micro aerial vehicles. *47th AIAA Aerospace Sciences Meeting Including the New Horizons Forum and Aerospace Exposition*, 1290. https://doi.org/10.2514/6.2009-1290

Saddington, A., Finnis, M., & Knowles, K. (2015). The characterisation of a gust generator for aerodynamic testing. *Proceedings of the Institution of Mechanical Engineers, Part G: Journal of Aerospace Engineering*, *229*(7), 1214–1225. https://doi.org/10.1177/0954410014548237

Sever, A. C. (2005). *Self-excited oscillations due to flow past slotted plate configurations* [PhD Thesis]. Lehigh University.

Smith, Z. F. (2018). *Micro air vehicle scale gust-wing interaction in a wind tunnel* [M.Sc Thesis]. University of Maryland.

Son, O., & Cetiner, O. (2017). Three-dimensionality effects due to change in the aspect ratio for the flow around an impulsively pitching flat plate. *Journal of Aerospace Engineering*, *30*(5), 04017053.

Son, O., & Cetiner, O. (2018). Force-motion phase relations and aerodynamic performance of a plunging plate. *Experiments in Fluids*, *59*(2), 1–11. https://doi.org/10.1007/s00348-017-2484-x

Viswanath, K., & Tafti, D. K. (2010). Effect of frontal gusts on forward flapping flight. *AIAA Journal*, *48*(9), 2049–2062. https://doi.org/10.2514/1.J050263

Watkins, S., Milbank, J., Loxton, B. J., & Melbourne, W. H. (2006). Atmospheric winds and their implications for microair vehicles. *AIAA Journal*, *44*(11), 2591–2600. https://doi.org/10.2514/1.22670

Watkins, S., Thompson, M., Shortis, M., Segal, R., Abdulrahim, M., & Sheridan, J. (2010). An overview of experiments on the dynamic sensitivity of MAVs to turbulence. *Aeronautical Journal*, *114*(1158), 485–492. https://doi.org/10.1017/s0001924000003973

Wei, N. J., Kissing, J., & Tropea, C. (2019b). Generation of periodic gusts with a pitching and plunging airfoil. *Experiments in Fluids*, *60*(11), 1–20. https://doi.org/10.1007/s00348-019-2815-1

Wei, N. J., Kissing, J., Wester, T. T., Wegt, S., Schiffmann, K., Jakirlic, S., Hölling, M., Peinke, J., & Tropea, C. (2019a). Insights into the periodic gust response of airfoils. *Journal of Fluid Mechanics*, *876*, 237–263. https://doi.org/10.1017/jfm.2019.537

Young, A. M., & Smyth, A. S. (2021). Gust–airfoil coupling with a loaded airfoil. *AIAA Journal*, *59*(3), 773–785. https://doi.org/10.2514/1.J059688

Zarovy, S., Costello, M., Mehta, A., Gremillion, G., Miller, D., Ranganathan, B., Humbert, J. S., & Samuel, P. (2010). Experimental study of gust effects on micro air vehicles. *AIAA Atmospheric Flight Mechanics Conference*, 7818.